MID TERM REPORT FOR GITEC-TWO
UIO group

G. Pedersen, H.P. Langtangen, H. Johnsgard and B. Gjevik
Department of Mathematics, University of Oslo, Box 1053, 0316 Oslo, Norway

1 Introduction

In the first GITEC project the UIO group performed a series of case studies concerning tsunami events in the Atlantic, the eastern Mediterranean and the Norwegian sea. During the project the focus was slightly shifted towards general model analysis and development. Preliminary Lagrangian run-up models and FE (finite element) techniques for Boussinesq equations were reported. Moreover, tests concerning the convergence and applicability of the standard long wave models were included in the case studies or carried out as separate tasks. Continuing this trend, we have spent the first year of GITEC-TWO mainly on model activities, even though the work on the 1969 tsunami outside Portugal has continued. All the model development and analysis rely heavily upon the experience from this and other case studies from the preceding project. In the second year more attention will be devoted to case studies. We will then first address a set of idealized, but challenging, cases before we proceed to exploit our new modeling tools and insight in the full studies of actual events. Even though we are not committed on this point in the work program, we hope to reach this stage within GITEC-TWO.

A small number of test cases have already been established, including wave generation and interaction with a shallow seamount, run-up on an idealized headland and wave propagation in two dimensional geometries corresponding to cross sections of the Portuguese coasts. Some of these problems are also addressed by the LDG.

The prolonged study of the 1969 tsunami, originating near the Gorringe Bank, is linked to the publication of a common paper [3] with the ICTE and the LDG. Due to the complexity of the problem and the diversity of the subtopics involved the paper has been substantially revised during GITEC-TWO before being finally accepted by the JGR. In particular a new study of convergence and non-hydrostatic effects has been included. This is further described in section 3. In addition a part of the study has served as a benchmark problem for verification and comparison of models at the LDG and the UIO.

It might seem surprising, but some of the properties of the most standard tsunami models are insufficiently documented in the literature. This is alarming since much of the tsunami work world wide still have to rely on the standard methods. Naturally,

many of the features will also be inherited by more advanced models. Facing this problem during the preceding project we have undertaken a study of the optical properties of FD (finite difference) and FE models, as well as on the influence of so called staircase (sawtooth) boundaries on the coastal response to incident waves. The results are summarized in section 4. Together with section 3 these topics form a fairly broad analysis on the shortcomings and accuracy of linear hydrostatic models.

The FE (finite element) model for the Boussinesq equations has been upgraded, analyzed and fully documented in the manuscript [7]. The evaluation and verification of the method are partly based on the test cases described above. More details are given in section 5.

Finally we describe the activity on run-up models in section 6. The FD Lagrangian model for run-up, employed under the first GITEC project, has been further developed, tested and documented in two journal articles. A comparison with results obtained by run-up models of the LDG, as well as inclusion of breaking waves, is under way. Moreover, a related, but more general, FE technique has been implemented in object oriented code and compared to analytical solutions as well as to the pre-existing FD method. So far, the tests are promising.

2 Formulation

Marking dimensional quantities by a star we introduce an orthogonal coordinate system with horizontal axes $ox^\star$, $oy^\star$ in the undisturbed water level and $oz^\star$ pointing vertically upwards. We specify the bottom according to $z^\star = -h^\star(x^\star, y^\star, t^\star)$, where the time dependence corresponds to a slide or bottom deformation due to an earthquake. Moreover, $\eta^\star$ is the surface elevation, $\vec{v}^\star$ and $\phi^\star$ the depth averaged horizontal particle velocity and velocity potential respectively. Employing h_0, the maximum depth for instance, as "vertical" length-scale and L as "horizontal" length-scale we then define non-dimensional variables

$$\left.\begin{array}{llll} x^\star = L^\star x, & y^\star = L^\star y, & t^\star = L^\star (g h_0^\star)^{-\frac{1}{2}} t, & h^\star = h_0 h \\ \eta^\star = \alpha h_0^\star \eta, & z^\star = h_0^\star z, & \vec{v}^\star = \alpha (g h_0^\star)^{\frac{1}{2}} \vec{v}, & \phi^\star = \alpha L (g h_0^\star)^{\frac{1}{2}} \phi \end{array}\right\} \qquad (1)$$

where g is the constant of gravity and α may be chosen as a characteristic amplitude. The choice of L varies; L may be chosen as a wavelength, as a characteristic length of the bathymetry or equal to h_0. In section 3, that concerns the 1969 tsunami at the Portuguese coast, we almost exclusively employ dimensional quantities. Here, as well as a few places elsewhere, the stars are omitted, but the units are explicitly stated.

2.1 Long wave equations

In Eulerian form the equations are best described with L as a wavelength. Assuming that the temporal depth variations are comparable to the amplitudes, it is also convenient to specify the time derivative of the depth as αq. Provided $\epsilon \equiv h_0^2/L^2$

is small the fluid motion is governed by the Boussinesq equations. With η and ϕ as dependent variables we obtain equations of the form ([15], [10])

$$\eta_t + q = -\nabla \cdot \vec{Q} \tag{2}$$

$$\phi_t + \frac{\alpha}{2}(\nabla\phi)^2 + \eta - \epsilon\left\{\frac{h}{2}q_t + \frac{h}{2}\nabla\cdot\left(h\nabla\phi_t\right) - \frac{h^2}{6}\nabla^2\phi_t\right\} = O(\epsilon^2, \epsilon\alpha) \tag{3}$$

where $\vec{Q}$ is given by

$$\vec{Q} = (h+\alpha\eta)\nabla\phi + \epsilon h\left(\frac{1}{6}\eta_t - q - \frac{1}{3}\nabla h\cdot\nabla\phi\right)\nabla h + O(\epsilon^2, \epsilon\alpha), \tag{4}$$

The subscript t denotes differentiation with respect to time and ∇ is the horizontal component of the gradient operator.

We have also employed another set of Boussinesq equations, based on $\vec{v}$ as dependent variable instead of ϕ. In (2) we then insert $\vec{Q} = (h+\alpha\eta)\vec{v}$, whereas (3) is replaced by the two components of the horizontal momentum equations, each having a structure very similar to (3). Omitting the terms of order ϵ we then obtain Airy's equations, whereas omission also of the order α terms yields the linear shallow water equations that are the basis of the simplest tsunami models. Further details concerning the equations and their relations are found in [10].

In the Lagrangian run-up models the factor α is most conveniently set to unity. Owing to the long wave assumption, we introduce a Lagrangian description by marking material *columns* of water by label coordinates (a,b). The relation between the Lagrangian coordinate a and Eulerian coordinates reads

$$\frac{\partial a}{\partial t} + \vec{v}\cdot\nabla a = 0,\ a(x,y,0) = a_0(x,y), \tag{5}$$

where $a_0(x,y)$ may be chosen as to obtain a domain of regular shape n in the (a,b) plane. Naturally, the other Lagrangian coordinate, b, fulfills a corresponding equation. A complete treatment of Lagrangian coordinates is found in [6]. In the present context, the main advantage of Lagrangian coordinates is the fixed computational domain that enables a simple and accurate treatment of the moving shoreline.

The continuity equation, that can be integrated once in time, reads

$$H\frac{\partial(x,y)}{\partial(a,b)} = V, \tag{6}$$

where $H \equiv h+\eta$ is the total depth, V is the volume per $da\times db$ and $\frac{\partial(\ ,\ )}{\partial(a,b)}$ denotes the Jacobian determinant. We note that equation (6) explicitly states mass conservation for a material water column. The momentum equations are employed with different expressions for the pressure term. In the hydrostatic case ($\epsilon = 0$) the x component reads

$$V\frac{\partial^2 x}{\partial t^2} = -H\frac{\partial(\eta,y)}{\partial(a,b)} = -\frac{\partial}{\partial a}\left(\frac{1}{2}H^2\frac{\partial y}{\partial b}\right) + \frac{\partial}{\partial b}\left(\frac{1}{2}H^2\frac{\partial y}{\partial a}\right) + V\frac{\partial h}{\partial x}. \tag{7}$$

We note that the rightmost expression for the pressure term is in conservative form.

2.2 Numerics

During the first half of the GITEC-TWO project we have performed much analysis on existing and new numerical techniques, which involves a considerable amount of manipulation of finite difference expressions. This work is facilitated by a simple notation as well as a number of standard formulas. Omitting the latter we report the former briefly. The approximation to a quantity f at a grid-point with coordinates $(\beta\Delta x, \gamma\Delta y, \kappa\Delta t)$ where Δx, Δy and Δt are the grid increments, is denoted by $f^{(\kappa)}_{\beta,\gamma}$. We introduce symmetric difference and average operators, δ_x and $^{-x}$ according to

$$\delta_x f^{(\kappa)}_{\beta,\gamma} = \frac{1}{\Delta x}(f^{(\kappa)}_{\beta+\frac{1}{2},\gamma} - f^{(\kappa)}_{\beta-\frac{1}{2},\gamma}), \quad (\overline{f}^{x})^{(\kappa)}_{\beta,\gamma} = \frac{1}{2}(f^{(\kappa)}_{\beta-\frac{1}{2},\gamma} + f^{(\kappa)}_{\beta+\frac{1}{2},\gamma}). \tag{8}$$

It is easily shown that these operators are commutative in all combinations. To abbreviate the expressions further we also group terms of identical indices inside square brackets, leaving the super- and subscripts outside the right bracket.

In all our numerical techniques we apply a time staggered grid in the sense that values for η or H, as well as x, y in the Lagrangian description, are specified at integral time steps, $n\Delta t$, whereas $\vec{v}$ and ϕ are sought at intermediate times, $(n-\frac{1}{2})\Delta t$. In (2) we treat the nonlinear term by an arithmetic average of η, while the convective term of (3), or the momentum equations, is represented by a geometric temporal average. For each time step this yields linear decoupled systems of implicit equations for η and ϕ, or $\vec{v}$, with a corresponding efficiency benefit both for FE and FD formulations. When the $O(\alpha, \epsilon)$ terms are omitted, and the mass matrices are lumped for FE formulations, we obtain a centered explicit scheme. On the other hand, for the hydrostatic equations in Lagrangian form we obtain an explicit scheme also in the non-linear case.

The spatial FD discretizations are based on the Arakawa C-grid for Eulerian equations, while a B-grid is used for Lagrangian formulations. Detailed descriptions are found in [10] and [5]. Herein, we present only the Eulerian scheme for $\alpha, \epsilon \to 0$. In terms of the formalism as outlined above it may be compactly expressed as

$$[\delta_t \eta = -\delta_x(\overline{h}^{x} u) - \delta_y(\overline{h}^{y} v)]^{(n+\frac{1}{2})}_{i,j}, \quad [\delta_t u = -\delta_x \eta]^{(n)}_{i+\frac{1}{2},j}, \quad [\delta_t v = -\delta_y \eta]^{(n)}_{i,j+\frac{1}{2}}, \tag{9}$$

where we have assumed that values for the depth are available at η nodes and the terms involving a time dependent bottom are omitted. From these equations we may easily eliminate the velocities by application of the difference operators δ_x, δ_y and δ_t. We then arrive at a scheme for the standard wave equation with variable coefficients. Moreover, if we assume temporal periodicity we may insert $\eta = \mathrm{Re}(\hat{\eta}(x,y)e^{-\mathrm{i}\omega t})$, to obtain

$$\delta_x(\overline{h}^{x}\delta_x\hat{\eta}) + \delta_y(\overline{h}^{y}\delta_y\hat{\eta}) + \tilde{\omega}^2\hat{\eta} = 0 \tag{10}$$

where $\tilde{\omega} \equiv \frac{2}{\Delta t}\sin\frac{\omega\Delta t}{2}$. This equation is the starting point for the analysis in section 4.

Concerning the FE methods we have paid particular attention to the relation to the FD formulations. Naturally, this depends on the element discretizations, of

which we employ a variety, as well as on the integration rules used in the generation of element matrices. Often we may observe that the result resembles a B- or C-grid FD formulation.

3 The 1969 case study

Most of the computations in [3] for the 1969 Portuguese event are based on shallow water theory that neglects the influence of non-hydrostatic (dispersive) and non-linear effects. This will first affect the initial surface elevation that is deduced from the sea bed deformation. In hydrostatic shallow water theory *rapid* bottom displacements are directly transferred to the surface, thereby introducing an unphysical as well as inconvenient discontinuity in the surface elevation. In our simulations this unwanted feature was avoided by a direct smoothening. However, a more accurate description of the response of the liquid to the sea bed motion will prevent the discontinuity in the first place and replace it by a comparatively steep gradient. Secondly, in view of the presence of regions with rapid variations in the initial surface elevation, the effect of dispersion must have some influence on the wave propagation, in deep water at least. For the rather low amplitude tsunami of 1969 nonlinear effects will primarily be important in large areas of very shallow water, as in river deltas and coastal marsh lands. Indeed, some of the important harbors at the Iberian coast are situated in or close to such areas. A reliable estimation of nonlinear effects in such sites requires a formidable amount of local analysis with high resolution models. Our partners at the LDG make progress on this topic at present. However, in the present section we will focus mainly on dispersion and grid refinement effects.

During the study of the 1969 tsunami we have performed a large number of tests on the importance of dispersion, nonlinearity and discretization errors. Herein we focus at a fresh study involving idealized two dimensional simulations.

In two dimensions (the vertical + 1 horizontal) the LDG has produced a fairly complete hydraulic response to the Okada source model by employing the program Nasa-Vof3D that solves the incompressible Navier-Stokes equations with a free surface [14]. The source is implemented by specifying a vertical velocity (sink/source distribution) at the bottom, with total periods of duration ranging from 1 to 20 seconds. All duration times gave virtually identical surface elevations – the subsequent results are based on 10 seconds. As shown in figure 1(a) the resulting surface elevation is very close to the bottom displacement, except for the discontinuity over the focal line that is replaced by a transition zone of about 18 km. Associated with this zone we still obtain a large content of short waves in the spectrum that will have bearing on the subsequent analysis of dispersion effects and discretization errors. It is also noteworthy that the maximum surface elevation is reduced almost 30% as compared to the bottom deformation, while the region of depression at the surface is substantially reduced.

We now turn to the discussion of non-hydrostatic effects during wave propagation. For plane waves on constant depth the dispersion relation may be written in the

generic form

$$c = c_0(1 - \gamma k^2 + O(k^4)), \quad \gamma = \frac{1}{6}h^2 + \frac{1}{24}(\Delta x^2 - c_0^2 \Delta t^2) \tag{11}$$

where Δx, Δt are the grid increments, k is the wave number, $c_0 = \sqrt{gh}$ is the shallow water wave celerity and the direction of wave advance is assumed to be parallel to the x-axis. We have incorporated both physical and numerical dispersion in such a manner that omission of the second term in γ yields the analytic dispersion relation for the Boussinesq equations, whereas omission of the first term corresponds to discrete solutions of the hydrostatic equations according to (9). Observing that discretization errors from the dispersion term are of order k^4, we then realize that keeping both terms in γ gives the wave celerity for numerical solutions of the Boussinesq equations.

Some useful observations follows immediately from (11) combined with geometrical optics that implies $k \sim h^{-\frac{1}{2}}$. The part of the difference $c - c_0$ that stems from real dispersion will then vanish in proportion to h in shoaling water, whereas the contribution from discretization errors will increase as h^{-1}. Naturally, in the limit $h \to 0+$ the latter result no longer applies because the optical description collapses and the wave length, however defined, does not approach zero. An indication of the validity range of the optics is given implicitly in figure 1; we may assume that geometrical optics is applicable as long as Green's law is valid. We may also extract some information concerning the evolution of a pulse in water of constant depth from (11). Assuming a generic initial condition of the form $\eta(x,0) = F(x/\lambda)$, where λ is a measure of the length of initial elevation, we find that the evolution of the wave shape is governed by the dimensionless time

$$\tau = \gamma c_0 t/\lambda^3 \tag{12}$$

that is a measure of the integrated effect of dispersion. This result is readily obtained from a Fourier integral or by rescaling the KdV equation belonging to the dispersion relation (11). The evolution of the initial pulse described above is given in figure 1(a) (λ set to 100 km) for different values of τ. The profiles are obtained by numerical solution of a KdV equation. With $h = 5$ km the action of physical dispersion over a distance of 200 km then yields $\tau = 0.83 \cdot 10^{-3}$. For comparison we note that *numerical* dispersion for $\sqrt{2}c_0\Delta t = \Delta x = 1$ km, over the same distance, corresponds only to $\tau = 4.2 \cdot 10^{-6}$. On the other hand, we may imagine that the pulse is conveyed to shallow water of depth $h = 10$ m, without any other change in shape than becoming shorter according to geometrical optics (length $\sim h^{\frac{1}{2}}$). Then, $\tau = 2 \cdot 10^{-3}$, that is the largest value in figure 1(a), corresponds to a propagation distance of no more than 4.3 km. The wave is affected by dispersion in two ways. First, the primary elevation decreases in height while the shape is altered through the evolution of a prolongated nose. An important consequence is the drastic reduction of the leading trough. In fact, in view of the actual propagation distances for the 1968 tsunami, the combined non-hydrostatic effects during generation and propagation make a leading depression virtually vanish. Thus, for the 1969 tsunami *the negative part of the Okadas source*

can hardly be directly observed at the coasts. Secondly a modulated wave train is separated from the leading pulse. The characteristics of this train are connected with the initial steep region above the fault.

Naturally, the importance of dispersive effects on a wave like the 1969 tsunami will inherit local variations according to the bathymetry and the orientation of the focal line. Still, we may construct a typical plane geometry by having a deep region with $h = 5000\,\mathrm{m}$ for positions $-200\,\mathrm{km} < x < 0\,\mathrm{km}$, a slope from $x = 0\,\mathrm{km}$ to $x = 190\,\mathrm{km}$, where the depth is $h = 10\,\mathrm{m}$, and finally another slope stretching to $x = 200\,\mathrm{km}$ where the depth vanishes. The latter region, that contains a long interval with very shallow water, will impose strong requirements on the numerical model. Invoking the initial condition as given in figure 1(a) we then solve the linear shallow water equations (linhyd), linearized Boussinesq equations (disp), Airy equations and the full Boussinesq equations for grid increments in the interval $5\,\mathrm{km} > \Delta x > 0.083\,\mathrm{km}$. In this context we employ a set of Boussinesq equations based on velocities as primary unknowns (see section 2). Simulations have also been performed for the inverse polarity as compared to figure 1(a) that corresponds to a 180° rotation of the source.

We start by examining the effect of dispersion. As shown in figure 1(a), inclusion of dispersion yields a significant wave train following the leading pulse, that is markedly decreased in height. This is confirmed by the actual 2-D simulations. Focusing on the amplitude we define $f = \eta_{\max}(h/h_m)^{\frac{1}{4}}/A_m$ where h_m, the depth in the source region, is taken to be 5000 m, A_m is the maximum surface elevation of the initial condition, $\eta_{\max}$ is the maximum of the right going wave and h is the depth at which the maximum is found. A constant value of f will correspond to fulfillment of the well known Green's law [8]. According to figure 1(b-c) omission of dispersion causes a 10-15%, say, overshot in the amplitude for the initial condition as given in panel (a), while the error is increased to 30-40%, say, when the polarity of the source is reversed. Other studies seems to agree with the prior, thereby indicating that the 40% error is some kind of worst case estimate. The arrival at the coast of the first peak is delayed a few minutes by dispersion. As expected, retaining the nonlinearity of the Boussinesq equations we observe little difference before the wave enters very shallow water ($h < 10\,\mathrm{m}$) where something like an undulatory bore starts to develop. This causes an increase in the amplitude. In addition the arrival time of the first peak is reduced by some minutes. However, the significance of these features depends crucially on the presence of large area with very shallow water as in this example, and is not properly resolved even for $\Delta x = 83\,\mathrm{m}$. It is also noteworthy that the nonlinear hydrostatic (Airy) equations predict breaking for the normal polarity source in rather deep water, even for the small amplitudes involved.

The convergence of the linear shallow water model is demonstrated in figure 1(d-e) where we observe that the standard resolution $\Delta x = 1\,\mathrm{km}$ yields good results for depths $h > 20\,\mathrm{m}$, say, and that even $\Delta x = 0.5\,\mathrm{km}$ becomes inaccurate for $h < 10\,\mathrm{m}$. Moreover, the convergence is poorer for the inverse polarity, at least as far as the maximum wave height is concerned. More encouraging is the fact that the numerical errors and the errors due to omission of the dispersive term are of opposite sign and

often of comparable magnitude.

Finally we remark that the performed computations are based on source parameters owing to the 1969 event and an idealized geometry corresponding to the gentler bottom slopes off the Iberian peninsula. For the steeper regions numerical dispersion, for instance, will have shorter time to develop and its effect will be reduced. Moreover, the results may be conveyed to other events and regions only with the utmost caution. In general, every tsunami case study will require some tests of its own.

4 Analysis of long wave models

4.1 Discrete optics

A key question for a researcher in wave theory is to what extent a given numerical procedure defines a virtual medium with properties that are analogous to those of the physical medium. In the present section we pursue this question by developing an optical theory for discrete solutions of finite difference or element methods, with emphasis on amplification and spurious behaviour in shallow water. Particularly, we seek a numerical counterpart to the well known Green's law, which states that the amplitude of a normally incident long wave in shallow water is proportional to $h^{-\frac{1}{4}}$, where h is the depth. There are several textbooks surveying this theory, for instance [8]. We devote most attention to the analysis of the standard long wave model, as described in section 2. However, we have established corresponding theories for dispersive equations and element discretizations on regular grids as well.

Periodic waves may propagate in a slowly varying medium without significant diffraction or loss of identity. There are several mathematical formulations available for such problems among which geometrical optics is the simplest. The basic idea is to assume a dominant harmonic behaviour with a phase function that inherits slowly varying derivatives. When also slow variation of the amplitude is taken into account we advance to the level of physical optics. The equations of physical optics, such as Green's law, are derived either by formal perturbation expansions, like the WKBJ method, or directly from energy considerations. We established an optical theory for discrete harmonic solutions directly from a WKBJ approach based on the assumption of a slowly varying medium. Then, starting with a non-trivial derivation of expressions for the discrete energy density and flux, we attempted to reproduce these results. In spite of problems concerning ambiguity we were partially successful. However, we leave out the rather long discussions and derivations associated with the energy aspects. A more complete description of the present topic is found in the manuscript [11] that can be made available at request.

We start from an ansatz

$$\zeta_{i,j} = A_{i,j} e^{\mathrm{i}\xi_{i,j}}, \tag{13}$$

where the fast variation (on the wavelength scale) is exhibited by $\xi_{i,j}$ only , while $A_{i,j}$ and the differences of ξ vary slowly. The wave number components, denoted by k and ℓ in the x and y directions respectively, may now be defined through differences of ξ.

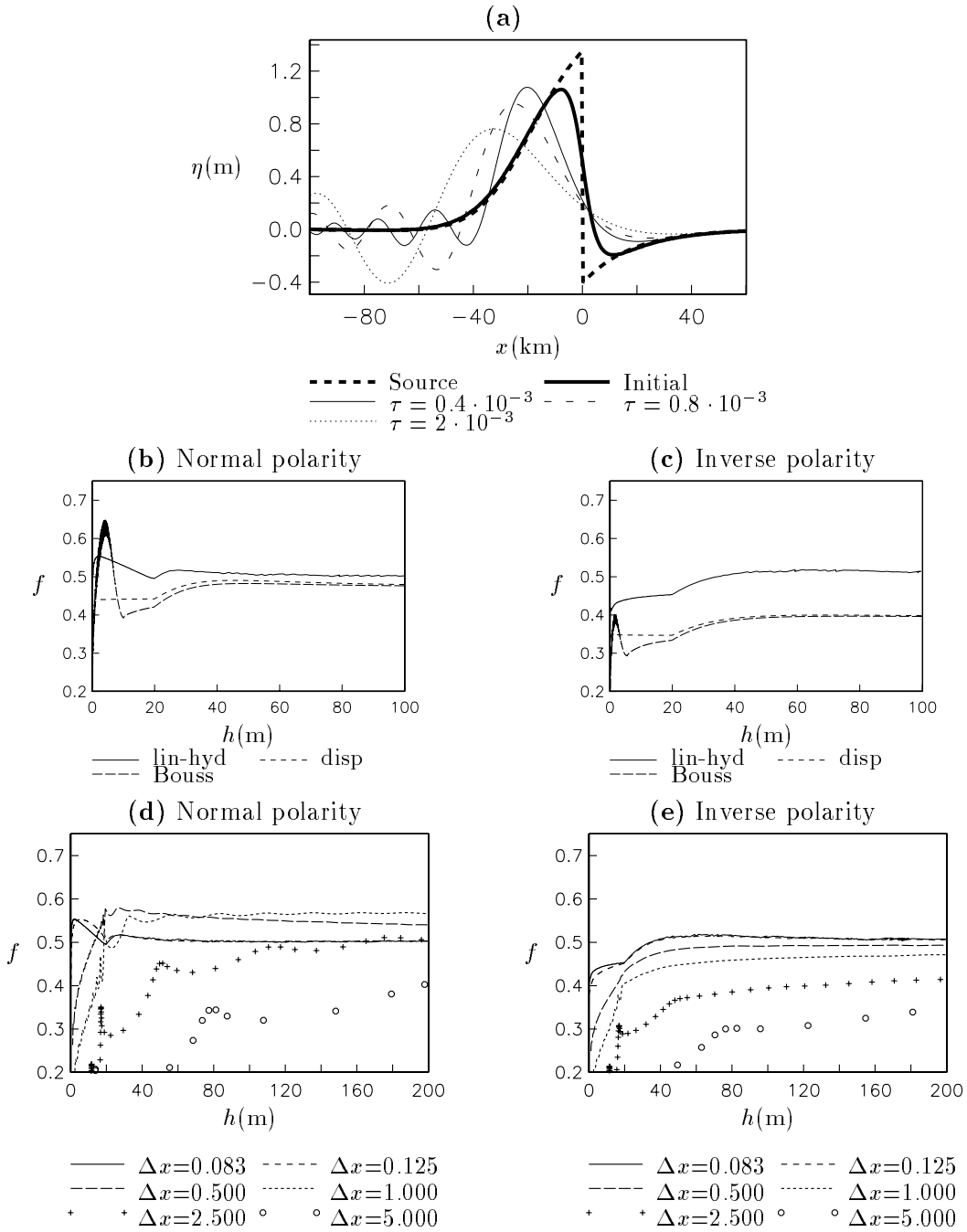

Figure 1: (a): Bold lines: Bottom deformation (dashed) and surface response (solid) Thin lines: evolution of pulse shape due to dispersive effects as explained in the text. (b,c): Amplitude of incident wave, normalized as explained in the text, for $\Delta x = 83\,\mathrm{m}$. (e,d): Convergence of linear hydrostatic model with grid increments in km and the depth in m.

Skipping the mathematical details we will instead sketch the premises and strategy for applying the WKBJ formulation to the numerical model. In the problem we may recognize three length scales. The rapid scale is given by a typical wavelength, that according to the scaling (1) is of order unity. We may characterize the long scale for depth and grid variations by $\frac{1}{\beta}$ where $\beta \sim h^{-1}\mathrm{d}h/\mathrm{d}x$, say. Finally we have the grid increment, Δx. To assure generality with respect to coarse grids we allow Δx to be of the same order as the wavelength. Substitution of (13) into the difference equation (10), followed by some manipulations, yields an expression where the fast variation is represented by algebraic expressions in the wave number components, whereas the slow variation manifest themselves through finite differences of depth, amplitude, wave numbers etc. This equation is then ordered simply by counting the number of "slow differences" in each term. Equating the leading order terms we reproduce geometrical optics, which expresses local fulfillment of the discrete dispersion relation, while the corresponding balance of terms of order β yields the physical optics. Now we observe that any second order discrete approximation to a slowly varying quantity will inherit relative errors of order $\beta^2\Delta x^2$. Since we neglect terms of $O(\beta^2)$ in physical optics we may then replace all such differences of slow variables by the derivatives to obtain a differential equation involving A, h etc. Naturally, this requires that analytic continuations exist for all discrete variables, including the unknowns A and ξ. Hence, A and ξ are prescribed as analytical functions, rather than discrete data distributed on a grid. Under extra assumptions the differential equation may actually be integrated in closed form (see below).

One important observation can be made from geometrical optics, or rather from the numerical dispersion relation, namely the existence of a minimum depth, h_c, for which real wave numbers may exist. A general lower bound is easily found to be

$$h_c \geq \frac{\Delta x^2 \Delta y^2 \tilde{\omega}^2}{4(\Delta x^2 + \Delta y^2)}, \tag{14}$$

where $\tilde{\omega} \equiv \frac{2}{\Delta t}\sin\frac{\omega\Delta t}{2}$.

The result of physical optics may be recasted into the conservative form

$$\nabla \cdot \left(A^2 h (C_x \tilde{k}\vec{\imath} + m_y^2 C_y \tilde{\ell}\vec{\jmath}) \right) = 0, \tag{15}$$

where $\tilde{k} \equiv \frac{2}{\Delta x}\sin(\frac{k\Delta x}{2})$, $C_x \equiv \cos(\frac{k\Delta x}{2})$ etc. We observe the analogy with the transport equation obtained from the differential equations. A case of particular interest is normally incident waves in a plane bathymetry, corresponding to $h = h(x)$ and $\ell = 0$. In this case (15) is easily integrated and the solution for A can be recasted into the very simple form

$$A = B(h - h_c)^{-\frac{1}{4}} \tag{16}$$

where B is a constant and h_c is the turning point depth, which is now given by $h_c = \tilde{\omega}^2\Delta x^2/4$. We note that (16) is a discrete generalization of Green's law and reproduces the latter in the limit $\Delta x \to 0$. When $h \to h_c^+$ the amplitude A becomes infinite and the physical optics collapses. As mentioned above, no real solution for k exists for

$h < h_c$. At $h = h_c$ we must thus expect a turning point with complete reflection of the incident wave. That reflection *does* occur may be demonstrated by matching the WKBJ solution to a local solution valid in the vicinity of the point. However, beyond noting that the local solution has the form $\zeta_j = (-1)^j C\mathrm{Ai}(\kappa(j\Delta x - d))$, where C, d and κ are constants, we omit the details. Naturally, the presence of a total reflection is also verified through direct numerical solution of the difference equations.

The formula (16) has been compared to exact discrete solutions, in the sense that they are obtained by solving the difference equation (10) directly. A convincing agreement is found, even for rather steep bottom gradients.

4.2 Run-up and staircase boundaries

As stated in the preceding subsections the optical theory collapses before the shoreline and cannot describe run-up. Consequently every harmonic retain finite length as well as amplitude. On the other hand, at the shoreline the governing equations inherit a singularity that may be expected to produce errors and artifacts in numerical solutions. The combination of the shoreline singularity with coarse grids, inaccurate digitized bathymetry and staircase boundaries calls for particular caution. In real case studies, as well as more idealized tests, we have observed a strong contamination by unphysical noise at the shore. Naturally, the use of staircase boundaries is a prime suspect concerning the noise production.

In the present section we focus on a simple geometry consisting of an offshore domain of constant depth combined with a plane slope extending to the shoreline. We align a Cartesian coordinate system with σ and γ axes normal and parallel to the shore respectively and obtain a bathymetry independent of γ. Moreover, we choose the offshore depth as h_0 and the slope length as L (see (1)).

A periodic incident wave is specified by its wavenumber $\vec{k}_\mathrm{i} = k(-\cos\psi\vec{\imath}_\sigma + \sin\psi\vec{\imath}_\gamma)$, which means that ψ is the angle of incidence.

4.2.1 The analytical solution

After elimination of $\vec{v}$ from the linear shallow water equations and separation of variables, according to $\eta = \zeta(\sigma)\exp(\mathrm{i}(k_\gamma\gamma - \omega t))$ we find

$$\frac{\mathrm{d}}{\mathrm{d}\sigma}\left(h\frac{\mathrm{d}\zeta}{\mathrm{d}\sigma}\right) + (\omega^2 - k_\gamma^2 h)\zeta = 0 \tag{17}$$

Provided $\frac{\mathrm{d}h(0)}{\mathrm{d}\sigma} \neq 0$ this equation inherits a regular singular point at $\sigma = 0$, which implies that one solution is finite as $\sigma \to 0^+$ whereas the other displays a logaritmic singularity. We note that for the singular ζ we obtain a finite, nonzero, limit for the flux hu. The requirement of finite ζ at $\sigma = 0$ may then be replaced by a no-flux condition, which has implications for the discrete procedure. For $\sigma < 1$ and normal incidence, $\psi = 0$, the non-singular solution of (17) reads $\zeta(\sigma) = C\mathrm{J}_0(2\omega\sqrt{\sigma})$ where J_0 is the Bessel function of zeroth order. There is a well known nonlinear generalization [1], that is employed in section 6. For oblique incidence the form of the solution

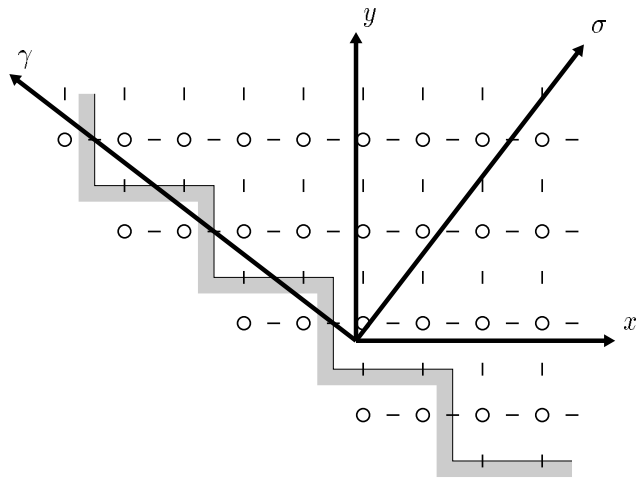

Figure 2: Definition sketch of staircase boundary ($N = 2$) and coordinate systems.

becomes slightly more complex, now involving the Kummer function. At $\sigma = 1$ the zeroth and first derivatives of nearshore solutions are patched to the offshore solution, that contains the incident and the reflected harmonic waves. A closer investigation of these solutions, including the discussion of some nontrivial features, is reported in [9].

4.2.2 Separation of variables in the discrete case.

We now assume that the grid is rotated an angle θ, in the clockwise direction, relative to the bathymetry. Moreover, we align the x, y coordinate system with axes parallel to the axes of the grid. If $\theta \neq 0, \frac{1}{2}\pi$ the shore then has to be represented as a "staircase boundary", consisting of segments being parallel to the x and y axes alternatively. Due to the simplicity of the bathymetry it is naturally to assume a grid with regular steps in the boundary, where a single increment in one direction is adjacent to a step in the other direction, counting a fixed number of increments. Without loss of generality we may then assume boundary segments of lengths Δy and $N\Delta x$ respectively, as displayed in figure 2 for the special case $N = 2$. To factorize a discrete solution it is not sufficient that the coefficients of the difference equation are independent of a given coordinate. In addition also the grid, including the representation of the boundary, must be invariant with respect to a shift in the coordinate. Thus we cannot employ separation in neither the γ,σ nor the x,y coordinates. Fortunately, the regularity of the sawtooth boundary enables a separation in the non-orthogonal system spanned by the x and γ axes. Hence, we proceed from (10) by the substitution

$$\hat{\eta}_{j,p} = e^{ik^{(\gamma)}(p-p_0)\Delta\gamma}\zeta_{1+j-j_0+(p-p_0)N}, \tag{18}$$

where j_0,p_0 is some reference node adjacent to a boundary segment parallel to the y-axis and $\Delta\gamma \equiv (\Delta y^2 + (N\Delta x)^2)^{\frac{1}{2}}$ is the grid increment in the γ direction. We note that that ζ_1 corresponds to the leftmost wet nodes.

From (10) we now obtain the ordinary difference equation

$$\left.\begin{aligned}\frac{h^{(s)}_{j-\frac{N}{2}}}{\Delta y^2}e^{-\mathrm{i}k^{(\gamma)}\Delta\gamma}\zeta_{j-N}+\frac{h_{j-\frac{1}{2}}}{\Delta x^2}\zeta_{j-1}+\left(\tilde{\omega}^2-\frac{h_{j+\frac{N}{2}}+h^s_{j-\frac{N}{2}}}{\Delta y^2}-\frac{h_{j+\frac{1}{2}}+h_{j-\frac{1}{2}}}{\Delta x^2}\right)\zeta_j\\ +\frac{h_{j+\frac{1}{2}}}{\Delta x^2}\zeta_{j+1}+\frac{h_{j+\frac{N}{2}}}{\Delta y^2}e^{\mathrm{i}k^{(\gamma)}\Delta\gamma}\zeta_{j+N}=0\end{aligned}\right\} \qquad (19)$$

where the quantity $h^{(s)}_{j-\frac{N}{2}}$ equals the actual depth when $j > N$ and zero otherwise. The latter case corresponds to the presence of the boundary segments parallel to the x-axis. At the offshore boundary we implement a combined input/radiation condition N times to close the system, which is then easily inverted by Gaussian elimination. For small N and flat bottom some progress can be made by analytical means as well.

4.2.3 Results

We start with the simplest case, namely $\theta = 0$, which implies $N = 0$. In the absence of a staircase boundary the problems concerning accuracy and singularity remain. So far, we have not discovered any particular difficulties associated with the singularity for $N = 0$. For fine grids the dominant error is due to the absence of a surface node at the shore. However, this is amended through a simple extrapolation. The results for a given set of parameters, corresponding to $\psi = 0°$, a slope length of 150 km and a wavelength in deep water equal to 50 km, are given in figure 3a. To make the relevance to real tsunami cases more readily accessible we retain dimensions in the figure. Proper convergence is not obtained until the grid size becomes a few hundred meters. We note that the error seems to increase roughly as $k^{4.5}$ for small Δx and that $\psi = 60°$ yields almost identical relative errors in the run-up as $\psi = 0°$.

An investigation of the case $N = 1$ (a one by one staircase boundary) reveals that no extra features will be introduced as compared to $N = 0$. The norm of the form function $|\zeta|$ is displayed in figure 3b for the case $\psi = 35°$, $k = 2\pi$ and $\Delta x = \frac{1}{25}$, which means that the length of the incident wave equals the length of the slope. We observe good overall convergence in spite of the coarse grid.

For $N \geq 2$ the numerical solution becomes more complex. In addition to the two independent solutions that corresponds to the incident and reflected waves, the difference equation (19) now possesses $N - 1$ decaying (evanescent) and $N - 1$ exponentially growing modes as $x \to \infty$. Naturally, the latter is discarded from the solution, whereas the former give rise to noise adjacent to the shore. In figure 3c we have displayed the result for the same parameters as in 3b. There is substantial degradation in performance of the numerical method relative to the case $N = 1$.

5 The FE Boussinesq solver

We have developed a fairly general finite element simulator for weakly nonlinear and dispersive water waves. The potential advantages of the finite element method, com-

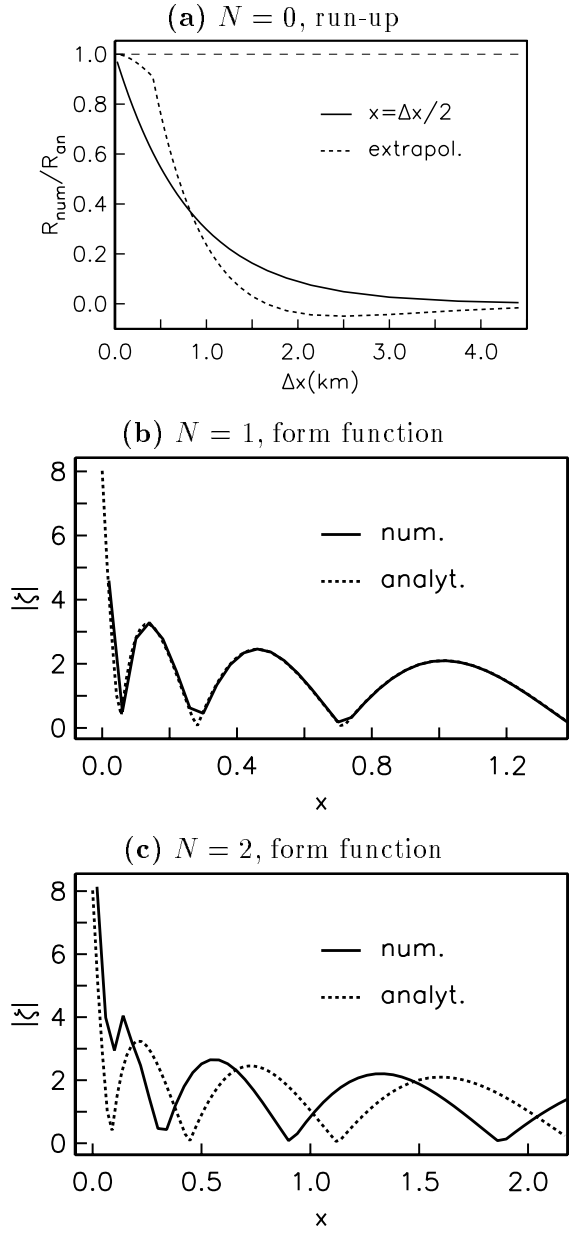

Figure 3: Comparison of numerical and analytical solutions as explained in the text.

pared to traditional finite difference schemes, are related to more accurate representation of coastal geometries, elimination of staircase boundaries, increased flexibility with respect to adaptive refinements etc., and simple generation of higher order spatial schemes. The disadvantages concern increased CPU-time (mostly due to the finite element assembly process), extra memory requirements, larger computer code, and less obvious means to develop ad hoc improvements of standard schemes.

The finite element simulator solves the Boussinesq equations, (2-3), with the surface elevation and the velocity potential as primary unknowns. For potential flow, this reduces the work by one third compared to the more standard approach where the velocity vector field is used as primary unknown. As mentioned in section 2, the equations are discretized in time by centered differences on a staggered grid. The spatial problems at each time level is then solved by a Galerkin finite element method. Our particular formulation has the no mass flux condition at the coastlines as natural boundary condition. The simulator is implemented in an object-oriented, yet efficient, fashion in C++, using the Diffpack library [2].

As an option, we have introduced correction terms in the equations. These (small) terms cancel certain terms in the local truncation error such that the time discretization of the linear hydrostatic equations becomes of fourth order. With a suitable choice of the time step (related to the dispersion parameter ϵ) and quadratic elements of size comparable to the depth, the numerical errors will then be of the same order as the residual $O(\alpha\epsilon, \epsilon^2)$ in the Boussinesq equations themselves.

A comprehensive analysis of the numerical accuracy has been performed by studying the error in the numerical wave velocity as a function of wave length, direction of wave advance, grid increments, grid distortion, consistent vs. lumped mass matrix representations etc. Only linear equations on constant depth are included in the theoretical analysis. We refer to a recently submitted journal article [7] for a detailed picture of the performance of various numerical strategies. One important result is that biquadratic elements loose their expected superiority when the elements become significantly distorted.

The finite element method has been investigated further in two idealized, but still challenging, test cases. The first case concerns an incoming plane wave on a bell-shaped beach, where the depth varies linearly in the vicinity of the beach. A contour plot, showing the reflection of an icident wave, is shown in figure 6, upper panel. Localized noise has been observed outside the headland, and this noise decreases as the curvature of the bell-shaped coastline decreases. Biquadratic elements seem to be less stable than linear or bilinear elements in this particular case.

The second application concerns the propagation of waves over a shallow seamount. This case is inspired by earthquake induced tsunamis at the Gettysburg seamount. Both the depth and the initial surface elevation have the shape of a bell function. Biquadratic elements and grids adapted to the bathymetry are much more efficient than finite difference methods on uniform grids in this case. As the water gap at the summit becomes very small (1 percent of the deep water depth), the superiority of biquadratic elements is somewhat reduced. Results for a plane wave passing over a

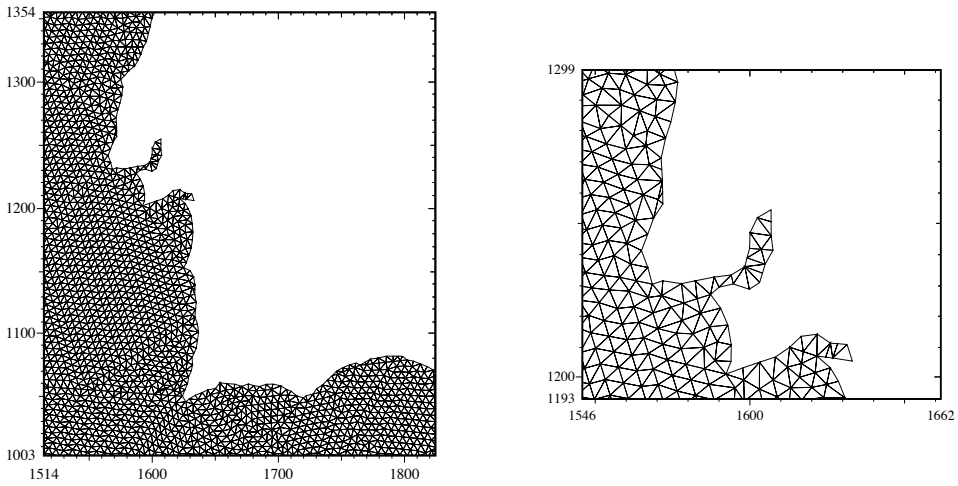

Figure 4: Left panel: Element mesh outside southern Portugal. Right panel: zoom of the Lisbon area. Axis units in km. (From U. Kolderup's Master thesis.)

very shallow seamount are displayed in figure 6, lower panel. The surface elevation is depicted by contours, while the seamount is shown as a wire plot.

We have also carried out some preliminary studies of the finite element model in the Atlantic ocean outside Iberia. Particularly, we have developed a technique for extracting coastline polygons from a depth matrix such that standard grid generation methods produce grids of acceptable quality close to the coastline, see figure 4. In this work we have also tested sponge layers and radiation conditions in the finite element model.

6 Lagrangian models

The UIO group has developed two sets of Lagrangian models to describe run-up of tsunamis at sloping beaches, based on nonlinear hydrostatic theory. A FD model, in several varieties due to different forms of the momentum equation, has been further developed since the first GITEC project. In addition mixed FE models are in progress. All models have been verified by comparison with two different analytical solutions as well as through intercomparison.

6.1 FD models

In addition to the comparison with analytical solution the FD procedure has been thoroughly tested through a small number of idealized test cases, including run-up on a headland (same geometry as in preceding section) and wave generation by a land slide into a fjord or lake. This work is documented in the articles [4] and [5].

The former also reports a preliminary plane shock model based on the inclusion of an artificial diffusion term. This model did not describe run-up of bores. Improved shock models that include run-up have been devised lately. However, there are still some conceptual problems concerning bores and run-up that need further elaboration. The results will be reported in the final report.

6.2 FE models

In accordance with the experience from the Eulerian FE models the Lagrangian technique is based on low order elements. Linear or bilinear trial functions defined on triangles and quadrilaterals, respectively, are employed for velocities. The surface elevation is constant over each element, which then yields a mixed formulation. The nodes are Lagrangian, in the sense that they move with the fluid velocity, whereas the shape functions are described in Eulerian coordinates. We model the continuity equation simply by requiring mass conservation for each element. For element i we then obtain

$$\eta_i A_i + \int_{E_i} h(x,y)\mathrm{d}x\mathrm{d}y = V_i,$$

where $A_i(t)$ is the area and V_i is the initial volume of the element.

A weak formulation for the momentum equation is then designed as to yield a natural boundary condition at the shoreline. Denoting the fluid domain by Ω and a weight function by W the x component reads

$$\int_\Omega W\ddot{x}\mathrm{d}x\mathrm{d}y = \int_\Omega \{(\eta+h)\frac{\partial W}{\partial x} + \frac{\partial h}{\partial x}W\}\mathrm{d}x\mathrm{d}y,$$

where $\ddot{x}$ is the particle acceleration. For quadrilaterals we obtain a representation of the pressure term that is very similar to the FD method based on the conservative formulation.

6.3 Comparison with analytical solutions

A set of particularly simple analytical solutions of the fully non-linear hydrostatic equations, concerning oscillations in parabolic basins, are found in [13]. We have generalized one of these slightly to allow a depth function $h(x,y) = h_0(y) - \alpha x^2$, where h_0 is any smooth function. The analytical solution then becomes

$$\eta = A(t) + B(t)x,\ u = U(t),\ B = B_0\sin(\omega t),\ \dot{U} = -B,\ A = -\frac{B^2}{4\alpha}$$

where $\omega = \sqrt{2\alpha}$. It can be shown that all our numerical techniques, including FE methods with non uniform grids, reproduce this solution, save for modifications of the relation between U and B and the value of ω according to $\frac{2}{\Delta t}\sin(\frac{1}{2}\omega\Delta t) = \sqrt{2\alpha}$. This provides a test of the coding rather than on the performance of the method due to the simple spatial distributions. All our code has undergone this test.

In 1958 Carrier and Greenspan [1] published an analytical treatment of the hydrostatic and fully nonlinear run-up on an inclined plane. The assumption of constant bottom slope enabled an ingenious transformation, using the Riemann invariants, to a linear problem. Recently the theory has been generalized to include run-up in channels with parabolic cross-sections [12]. We will not go much into the particulars of the theory, but focus on one fundamental solution only, namely the standing wave oscillation. This solution is of fundamental importance and is closely related to the linear solutions in section 4. Moreover, it allows us to study the numerical reproduction of waves that are arbitrarily steep at the shoreline, even to the point of breaking. According to our experience this is a more challenging test for Lagrangian models than simulations involving large run-up distances, but small wave steepness.

Assuming $h^\star = \nu x^\star$ and a characteristic time scale, T, we select typical length scales according to

$$L = gT^2\nu, \quad h_0 = gT^2\nu^2 \tag{20}$$

which gives $h = x$. Carrier and Greenspan arrived at the linear wave equation:

$$\frac{\partial}{\partial\sigma}\left(\sigma\frac{\partial\phi}{\partial\sigma}\right) - \sigma\frac{\partial^2\phi}{\partial\lambda^2} = 0, \tag{21}$$

where the transformation to the physical quantities can be expressed as:

$$\left.\begin{aligned} u &= -\sigma^{-1}\tfrac{\partial\phi}{\partial\sigma}, \quad \eta = \tfrac{1}{4}\tfrac{\partial\phi}{\partial\lambda} - \tfrac{1}{2}u^2 \\ t &= \tfrac{1}{2}\lambda + u, \qquad x = -\tfrac{1}{4}\tfrac{\partial\phi}{\partial\lambda} + \tfrac{1}{16}\sigma^2 + \tfrac{1}{2}u^2. \end{aligned}\right\} \tag{22}$$

Choosing T as to give a nondimensional frequency equal to 2 we may write a standing wave solution of (21) according to:

$$\phi = A\mathrm{J}_0(\sigma)\cos\lambda \tag{23}$$

where J_0 is the Bessel function of zeroth order and A is an amplitude factor. For $A > 1$ the transformations in (22) become multivalued as an indication of wave breaking. We obtain the solution in the physical plane by converting the algebraic equations in (22) by means of an iterative solver. Combining this solver with a Runge-Kutta technique we may also obtain particle trajectories corresponding to the Lagrangian description.

We have performed simulations in a basin of length 10 and different amplitudes A for the FE and the non conservative, as well as the conservative, FD formulations (see (7)). Different aspects of the solution for the high amplitude $A = 0.95$ are displayed in the various panels of figure 5. In panel (a) we have compared the surface elevations for comparatively coarse grids. A closer investigation of the results reveals that the largest errors are generally found at the shoreline. Hence we focus on the shoreline motion in panel (b) for the non conservative FD method. We observe close convergence even though we have a "near cusp" in the analytical solution. All the other formulations do also converge, though at somewhat different rates. When an

analytical solution is available the convergence rate should always be investigated more rigourously. This is done in panel (c) where the error itself, relative to Δa^2, is depicted. Around the time of 'near breaking' we often obtain only what seems, after a closer analysis, to be a $\Delta a^2 \ln \Delta a$ convergence. Such a behaviour can be observed, more or less clearly, for all methods. For practical purposes this convergence rate may be considered as quadratic. Still it must be noted that lumping of the FE method at the shore produces spurious oscillations that yields an even slower convergence. However, the rate is still faster than linear. A direct comparison between the different methods is found in panel (d). We observe that the consistent FE formulation is clearly superior, whereas the two FD techniques are more or less equivalent.

A more complete treatise of the comparsion with the standing wave solution is given in an internal report that can be made available at request.

References

[1] Carrier, G.F. and Greenspan, H.P. 1958. Water waves of finite amplitude on a sloping beach. *J. Fluid Mech.* **4**, 97-109.

[2] The Diffpack WWW home page.
URL: `http://www.oslo.sintef.no/diffpack`.

[3] Gjevik B. *et al.*, 1997 Modeling tsunamis from earthquake sources near Gorringe Bank southwest of Portugal. *accepted by the JGR*

[4] Johnsgard H. & Pedersen G. 1997 Slide Generated Waves in Near-Shore Regions. A Lagrangian Description. *Phys. Chem. Earth,* **21**-12, 45-49.

[5] Johnsgard H. & Pedersen G. 1997 A numerical model for three-dimensional run-up. *Numerical Methods in Fluids* **24**, 913-931.

[6] Lamb, Sir H., Hydrodynamics.

[7] Langtangen, H.P. and Pedersen, G. 1996 Computational Models for Weakly Dispersive Nonlinear Water Waves. *Submitted*

[8] Mei, C.C., 1989 The applied dynamics of ocean surface waves. *Advanced Series on Ocean Engineering* Vol.**I**, 740 pp. World Scientific, London.

[9] Pedersen, G. 1985 Run-up of periodic waves on a straight beach. *Preprint Ser. Dept. of Maths., University of Oslo* **1/85**

[10] Pedersen G. 1988 On the numerical solution of the Boussinesq equations. *University of Oslo, Research Report in Mechanics* **88–14**

[11] Pedersen G. 1997 An optical theory for discrete media. *In progress.*

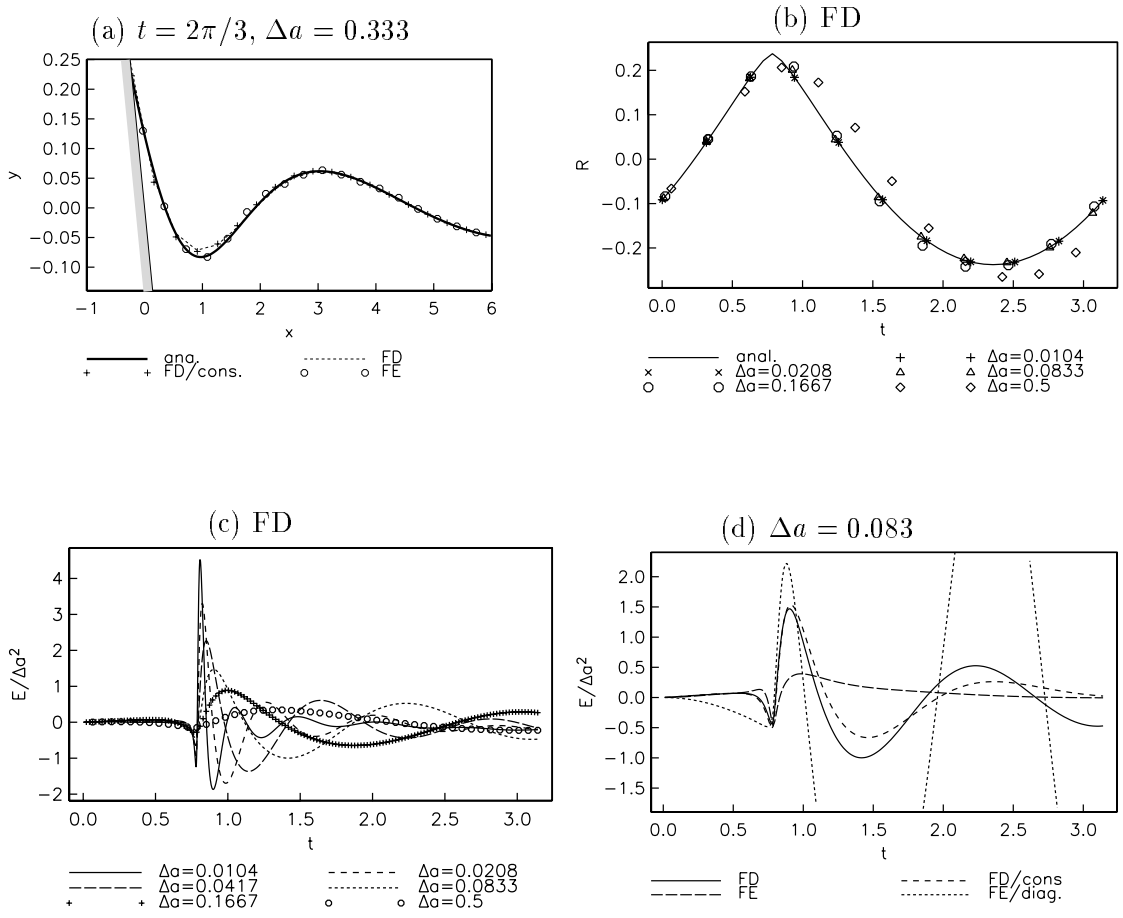

Figure 5: Comparison with analytical solution for run-up of standing waves, as explained in the text.

[12] Pelinovsky E., Kozyrev O. & Troshina E. 1995 Tsunami runup in a sloping channel. *Int. Workshop on long wave modelling. Seattle.*

[13] Thacker, W.C. 1981. Some exact solutions to the nonlinear shallow-water wave equations. *J. Fluid Mech.* **107**, 499-508.

[14] Torrey M.D. et al. 1987 NASA-VOF3D: a three-dimensional computer program for incompressible flows with free surfaces. Los Alamos National Laboratory, **LA1100-9MS**.

[15] Wu T.Y. 1981 Long waves in ocean and coastal waters. *Proc. ASCE, J. Eng. Mech. Div.* **107**,EM3,501–522

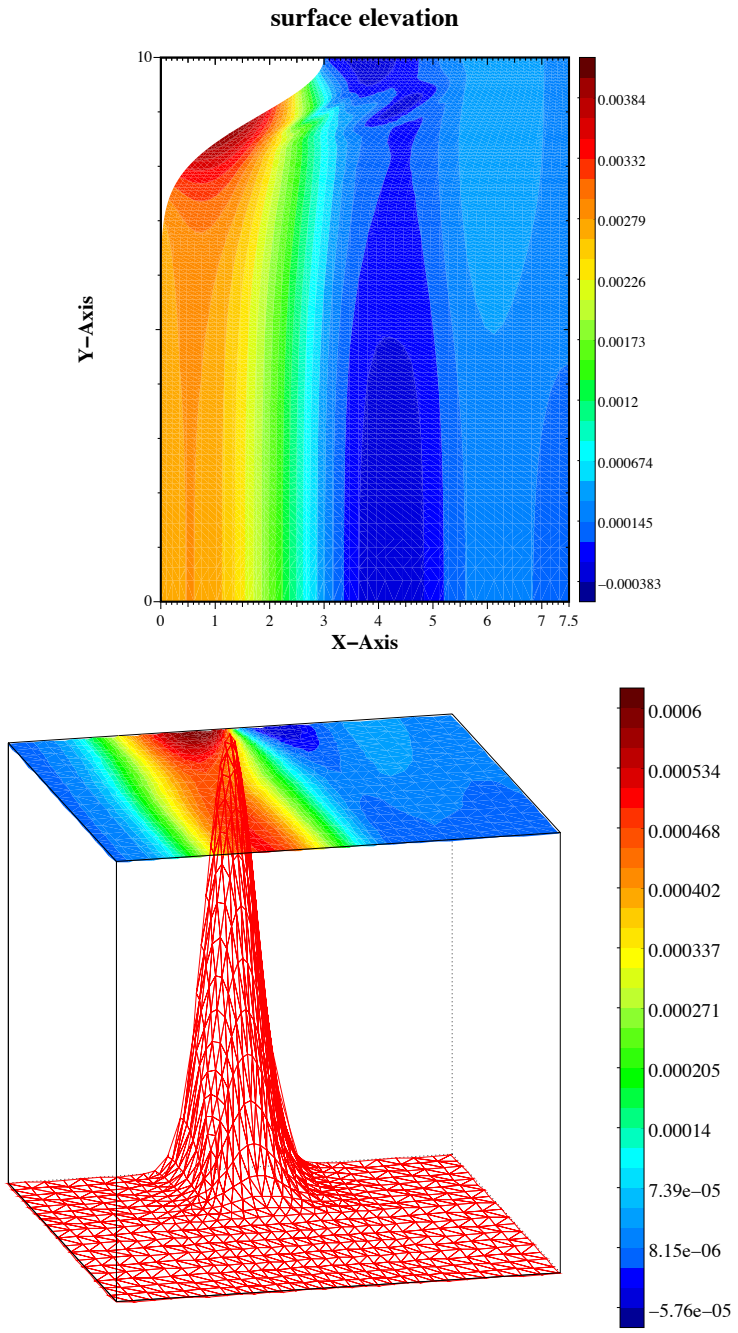

Figure 6: Boussinesq solutions for test cases. Upper panel: Snapshot of the surface elevation of a wave impinging on a headland. Lower panel: Focusing of a plane wave after passing a very shallow seamount.